Three-Dimensional Topological Ferroelectrics

Haohao Sheng,[1,2] Sheng Zhang,[1,2] Zhong Fang,[1] Hongming Weng,[1,3] and Zhijun Wang[1,3,*]
[1]Beijing National Laboratory for Condensed Matter Physics, and Institute of Physics, Chinese Academy of Sciences, Beijing 100190, China
[2]University of Chinese Academy of Sciences, Beijing 100049, China
[3]Condensed Matter Physics Data Center, Chinese Academy of Sciences, Beijing 100190, China

(Received 29 March 2026; accepted 23 September 2026; published 4 November 2026)

Three-dimensional topological ferroelectric (3D-TFE) insulators, in which topological and ferroelectric orders naturally coexist, enable field-controlled spintronic devices. In this Letter, we predict a previously unknown structure of bismuth monohalides Bi_4X_4 (X = Br, I), denoted the γ phase, and demonstrate that it is an ideal 3D-TFE insulator. Systematic first-principles calculations confirm the stability and synthesizability of γ-Bi_4X_4. Although the noncentrosymmetric γ phase crystallizes in the space group $Cmc2_1$ with no symmetry-based classifications or indicators, the nontrivial topology can be characterized by the nonzero spin Chern number. Moreover, the z-direction polarization can be switched by interlayer sliding with a small energy barrier. Finally, we design an electrically controlled spin-filter device that can generate a switchable spin-polarized current. Combining a single-phase crystal, a sizable band gap, and robust band topology against ferroelectric switching, these bismuth monohalides serve as a prototype of intrinsic 3D-TFE insulators, providing an ideal platform for realizing new nonvolatile functionalities in spintronic devices.

DOI: 10.1103/nwyq-3t1f

Introduction—Three-dimensional (3D) topological insulators [1–7] and topological crystalline insulators [8–10] exhibit emergent gapless surface or edge states protected by the bulk band topology, offering a material platform with unprecedented electronic properties. Owing to spin-momentum locking and suppressed backscattering, these boundary modes enable robust, low-dissipation charge and spin transport that has attracted intense interest for spintronic applications [11–13]. When such nontrivial topological states coexist with ferroelectric (FE) order, the resulting phase is referred to as a topological FE insulator. These metallic boundary modes can create an intrinsic short-circuit condition that strongly prevents the depolarization field. Most interestingly, the topological boundary modes become controllable by an external electric field.

To date, research on topological FE insulators remains at an early stage: most studies focus on two-dimensional (2D) systems with several key challenges unresolved, whereas intrinsic 3D topological FE (3D-TFE) insulators remain lacking. First, many efforts focus on 2D heterostructures with FE switching of topological states, such as In_2S_3/In_2Se_3 [14], CuI/In_2Se_3 [15], and $MnBi_2Te_4/In_2Te_3$ [16]. However, these systems possess very small band gaps (below 0.055 eV), making them susceptible to thermally activated carriers and electrical breakdown. Moreover, these heterostructures are difficult to realize experimentally due to the need for precisely engineered and lattice-matched interfaces [17,18]. Next, the nontrivial topological state of several 2D topological FE insulator candidates does not survive across the entire FE switching pathway, e.g., α-Bi monolayer [19–24]. In other words, a gapless phase transition point appears along the FE switching pathway, introducing unwanted metallic states and thereby undermining reproducible, nonvolatile FE devices. Finally, for 3D systems, only a few candidates have been theoretically proposed, yet all of them critically rely on external tuning to realize the topological FE insulator state, such as strained $CsPbI_3$ [25], the antiferroelectric KMgBi family [26,27], and SnTe during its FE phase transition [28]. No intrinsic 3D candidate has been reported yet. In order to utilize topological FEs for designing nonvolatile devices, it is essential to discover intrinsic 3D-TFE insulators with sizable band gaps and robust band topology.

Sliding ferroelectricity has been introduced [29–31], and sliding-induced topological FE metals have been reported in the T_d phases of the van der Waals (vdW) layered compounds $MoTe_2$ and WTe_2 [32–36]. FE switching in their bilayers has been observed experimentally [37,38]. In addition, the family of vdW layered bismuth monohalides Bi_4X_4 (X = Br, I) has attracted considerable attention. Experimentally synthesized members include low-temperature α-Bi_4I_4 [39,40], high-temperature β-Bi_4I_4[39,40], and α-Bi_4Br_4 (denoted the α' phase for clarity) [41,42]. The nontrivial band topology of their monolayers was first theoretically predicted in Ref. [43]. Subsequently, the topological properties of their bulk crystals have been

*Contact author: wzj@iphy.ac.cn

 © 2026 American Physical Society

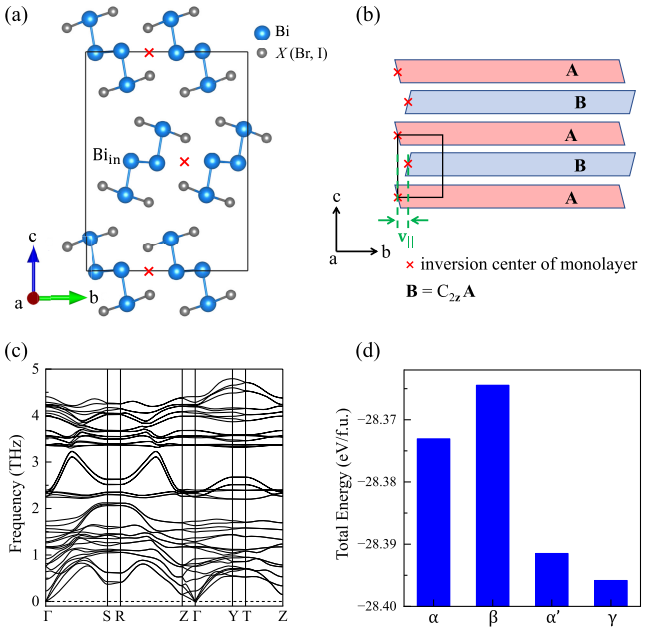


FIG. 1. Crystal structure and stability of γ-Bi_4Br_4. (a) Crystal structure of the γ phase. a, b, and c represent the conventional cell vectors. The red crosses "x" indicate the inversion centers of the individual layers. (b) Schematic plot of van der Waals ABAB $\cdots$ stacking. (c) Phonon spectrum. (d) Total energies per formula unit for different structures of Bi_4Br_4.

intensively studied [44–53]. The topological edge states have been observed by various experimental techniques, including angle-resolved photoemission spectroscopy [54], scanning tunneling microscopy (STM) [55], and microwave impedance microscopy [56]. Recently, the robust helical edge modes have been utilized as spin sensors for spin-resolved STM imaging [57]. However, all of these known bulk phases are centrosymmetric and consequently lack FE polarization in Bi_4X_4.

In this Letter, we predict a new γ phase of Bi_4X_4 and demonstrate that it is an ideal 3D-TFE insulator. First, phonon spectra, *ab initio* molecular dynamics simulations, and convex-hull analysis confirm the stability of γ-Bi_4X_4 and establish γ-Bi_4Br_4 as the ground state among all known phases. Second, the S_z spin Chern number (SCN) is calculated to be $C_{S_z} = 2$, indicating the spin-resolved topology of a 3D quantum spin Hall insulator (QSHI) state. Third, the z-direction polarization is switched by interlayer sliding. The natural coexistence of topological and FE orders in single-phase γ-Bi_4X_4, together with a sizable band gap and robust topology, enables field-controlled spintronic devices. Finally, we propose an electrically controlled spin-filter device in a bilayer film.

Crystal structure and stability—The new 3D γ-Bi_4X_4 structure is shown in Fig. 1(a). It is formed by a vdW stacking of the Bi_4X_4 monolayers (lying in the x-y plane) along the z direction. As illustrated in Fig. 1(b), two adjacent layers are related by a C_{2z} symmetry, forming an AB stacking arrangement. The sliding vector $\mathbf{v}_{||}$ is defined as the in-plane difference between the inversion centers of the adjacent layers. After relaxation, $\mathbf{v}_{||} = (0.00, 0.22)$ and $(0.00, 0.23)$ (with respect to the in-plane lattice vectors of the conventional cell) are obtained for γ-Bi_4Br_4 and γ-Bi_4I_4, respectively. Details of the calculation methods are provided in Sec. A of Supplemental Material (SM) [58]. The γ phase breaks inversion symmetry and belongs to the nonsymmorphic space group (SG) $Cmc2_1$, which contains mirror M_x, screw rotation $\tilde{C}_{2z} \equiv \{C_{2z}|0, 0, 0.5\}$, and glide mirror $\tilde{M}_y \equiv \{M_y|0, 0, 0.5\}$ symmetries. It is worth noting that the γ phase is an orthorhombic structure, with two layers in a conventional cell. Therefore, every other layer is well aligned in the z direction, which is quite different from the reported experimentally synthesized α'-Bi_4Br_4 [41,42] (Sec. B of SM [58]). Thus, we suggest that this structural distinction can be observed in scanning transmission electron microscopy (STEM).

Phonon spectrum calculations show no imaginary modes in Fig. 1(c), confirming that γ-Bi_4Br_4 is dynamically stable. *Ab initio* molecular dynamics simulations further confirm its thermal stability (Sec. C of SM [58]). Additionally, its formation energy above the convex hull is 0.033 eV/atom, indicating that γ-Bi_4Br_4 is likely experimentally synthesizable. Moreover, γ-Bi_4Br_4 is the ground state among all known phases, as shown in Fig. 1(d). For Bi_4I_4, however, the results show that the α phase has the lowest energy among these phases (Sec. D of SM [58]), consistent with the experimentally observed low-temperature phase. Nevertheless, the computed phonon spectrum shows that γ-Bi_4I_4 is also dynamically stable. As the Bi_4X_4-family compounds of the γ phase share the same properties, we take Bi_4Br_4 as an example in the main text.

Band structure and topology—From the Perdew-Burke-Ernzerhof band structure in Fig. 2(b), γ-Bi_4Br_4 exhibits an indirect band gap of 0.5 eV. Upon including spin-orbit coupling (SOC), the gap E_g is significantly reduced to 0.15 eV, as shown in Fig. 2(c). From the weight of the Bi_{in} p orbitals, we can clearly see that SOC induces the band inversion of two pairs of doubly degenerate bands along the entire Y-T line, indicating the potential nontrivial topology. As SG $Cmc2_1$ has no symmetry-based classifications, the nontrivial topology of γ-Bi_4Br_4 cannot be simply indicated by any symmetry eigenvalues.

Then, we demonstrate that the band topology is characterized by the S_z SCN. We perform spin-resolved Wilson-loop calculations to compute the SCN in a spinful system [75–78]. First, using the S_z spin operator, one can separate the occupied states into two spin subspaces. The projected spin operator is given by $PS_zP \equiv (\hbar/2)P(\mathbf{k})\hat{\sigma}_z P(\mathbf{k})$, where $P(\mathbf{k})$ is the projector onto the occupied energy bands. The eigenvalues of the projected spin matrix are presented in Fig. 2(d) and are well separated. Then, we calculate the one-dimensional Wilson loops for the upper spin bands [black dashed box in Fig. 2(d)] and obtain the spin-resolved Wannier

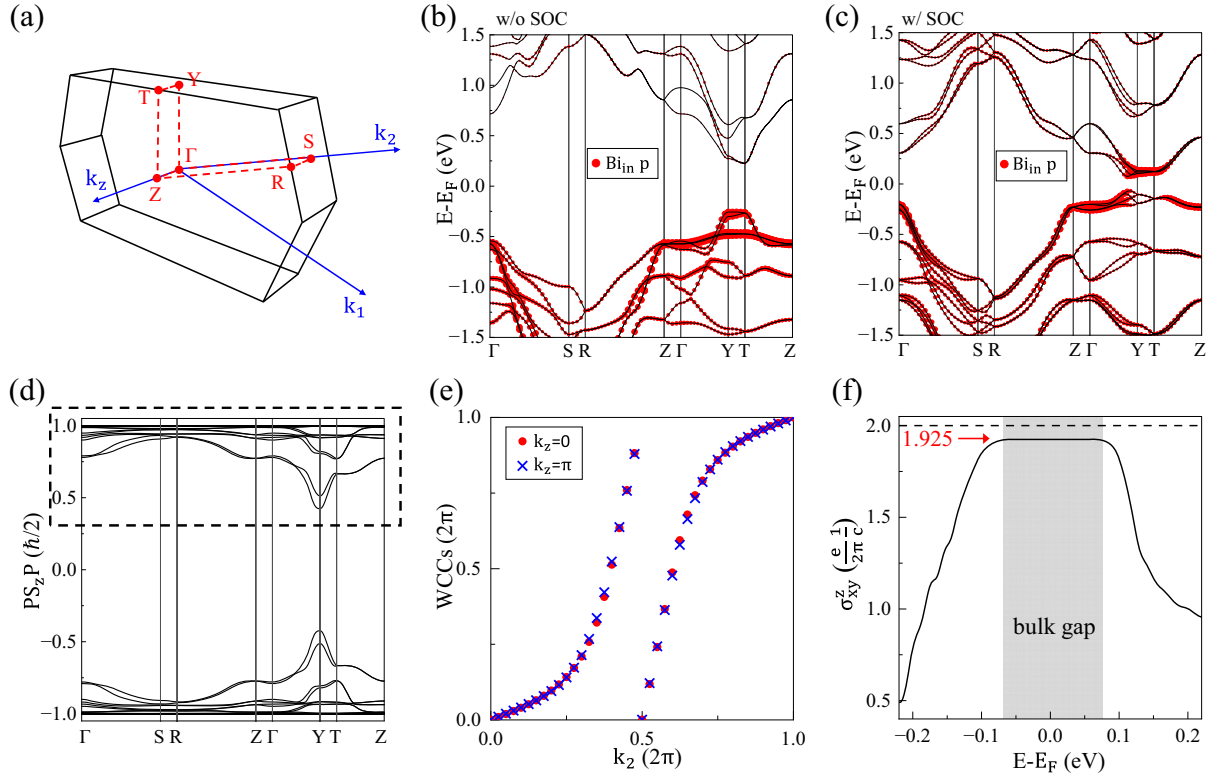


FIG. 2. Electronic structure, spin spectrum, and 3D QSHI state of γ-Bi_4Br_4. (a) Primitive Brillouin zone and high-symmetry k-points. Electronic band structures (b) without (w/o) SOC and (c) with (w/) SOC. The size of the red dots represents the weight of the Bi_{in} p orbitals. Here, Bi_{in} denotes the middle Bi atoms in each layer, as shown in Fig. 1(a). (d) Spin spectrum obtained from the eigenvalues of the projected spin matrix PS_zP. The black dashed box indicates the upper spin bands. (e) The k_1-directed Wilson loops of the upper spin bands. The resulting Wannier charge centers (WCCs), summed over all Wannier bands, are plotted as a function of k_2 on the $k_z = 0$ (red dots) and $k_z = \pi$ (blue crossing points) planes. (f) Intrinsic bulk spin Hall conductivity σ^z_{xy} as a function of chemical potential.

charge centers (WCCs; phases of the eigenvalues of the Wilson-loop matrices). The evolution of the WCCs shows that the partial Chern number of the upper spin bands is $C^+_{S_z} = 2$ for the $k_z = 0$ plane (red dots) and the $k_z = \pi$ plane (blue crossing points) in Fig. 2(e). Time reversal symmetry enforces $C^-_{S_z} = -2$ for the lower spin bands. We find that the SCN is $C_{S_z} = (C^+_{S_z} - C^-_{S_z})/2 = 2$ for all k_z planes, indicating the spin-resolved topology of a 3D QSHI state [78,79].

The SCN $C_{S_z} = 2$ produces a *topological* contribution to the spin Hall conductivity (SHC) of $2\{(e/2\pi)[1/c]\}$ in the 3D bulk, where c is the lattice constant in the z direction [78]. We calculate the *intrinsic* SHC σ^z_{xy} using the Kubo formula [80,81],

$$\sigma^z_{xy} = \frac{\hbar}{2e}\frac{e^2}{\hbar}\int_{\mathrm{BZ}}\frac{d^3k}{(2\pi)^3}\sum_n f_n(\mathbf{k})\Omega^z_{n,xy}(\mathbf{k}),$$

$$\Omega^z_{n,xy}(\mathbf{k}) = 2\hbar\sum_{m\neq n}\frac{-2\,\mathrm{Im}[\langle u_{n\mathbf{k}}|\hat{J}^z_x|u_{m\mathbf{k}}\rangle\langle u_{m\mathbf{k}}|\hat{v}_y|u_{n\mathbf{k}}\rangle]}{(\varepsilon_{n\mathbf{k}} - \varepsilon_{m\mathbf{k}})^2}, \quad (1)$$

where $\hat{J}^z_x = \frac{1}{2}\{\hat{S}_z, \hat{v}_x\}$ is the spin current operator; $\hat{S}_z = (\hbar/2)\hat{\sigma}_z$ is the spin operator; $\hat{v}_x = (1/\hbar)[\partial H(\mathbf{k})/\partial k_x]$ is the velocity operator; n and m are band indices running over all valence and conduction bands; $|u_{n\mathbf{k}}\rangle$ and $\varepsilon_{n\mathbf{k}}$ are the eigenstates and eigenvalues, respectively; $f_n(\mathbf{k})$ is the Fermi-Dirac distribution function; and BZ denotes the first Brillouin zone. As shown in Fig. 2(f), σ^z_{xy} exhibits a plateau of $1.925\{(e/2\pi)[1/c]\}$ within the band gap. Our results demonstrate that γ-Bi_4Br_4 hosts a 3D QSHI state with a nearly quantized SHC, which is calling for experimental verification.

Bulk polarization and ferroelectricity—Polarization is allowed in γ-Bi_4Br_4 due to the absence of inversion symmetry. The z-direction (out-of-plane) polarization is calculated to be 3.07×10^{-3} C/m^2 in the 3D bulk (2.89×10^{-3} C/m^2 for Bi_4I_4), which is comparable to the reported values of typical vdW stacked T_d-phase FEs (such as 2.4×10^{-3} C/m^2 for ZrI_2 [82]). To explore FE bistability and switching pathways, we calculate the total energy as a function of $\mathbf{v}_{||}$, as shown in Fig. 3(a). Two FE phases with opposite polarizations [FE1: $\mathbf{v}_{||} = (0.00, 0.22)$; FE2: $\mathbf{v}_{||} = (0.50, 0.28)$], which are related by inversion, are obtained. As depicted by the red dashed line, the FE switching can be realized by interlayer sliding. The energy profile and the polarization evolution along the pathway are plotted in Figs. 3(b)

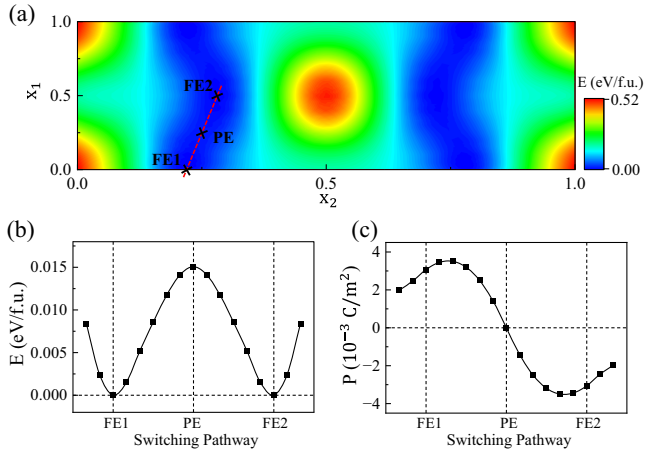


FIG. 3. Ferroelectric polarization and switching of γ-Bi_4Br_4. (a) Total energies per formula unit relative to the energy of the FE phases as a function of the interlayer sliding vector $\mathbf{v}_{||} = (x_1, x_2)$. The FE switching pathway is marked by the red dashed line. (b) Energy profile and (c) polarization evolution along the pathway. PE denotes the intermediate paraelectric phase.

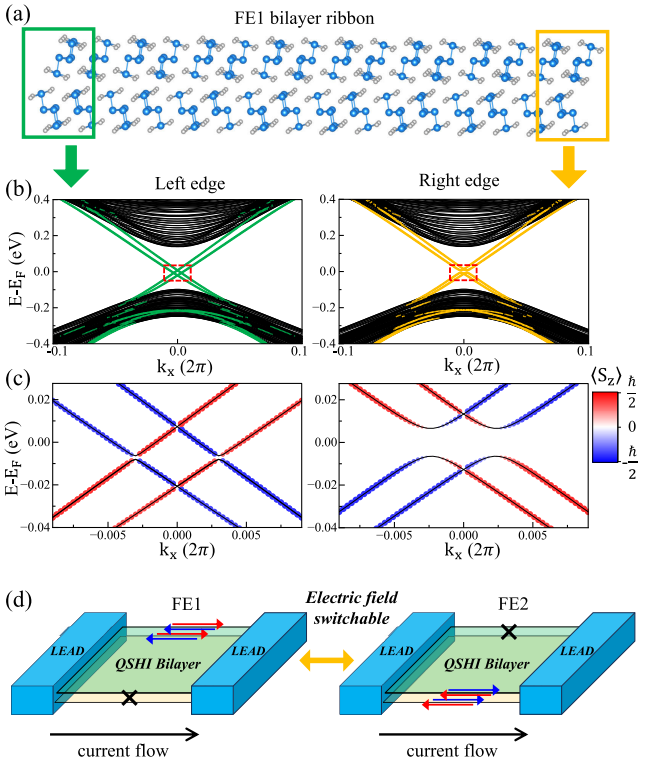


FIG. 4. Topological edge states and electrically controlled spin-filter device in the π bilayer of γ-Bi_4Br_4. (a) Crystal structure of the FE1 bilayer ribbon. (b) Band structures with SOC of the FE1 bilayer ribbon. The left-edge states (green dots) and the right-edge states (orange dots) are shown in the left and right panels, respectively. (c) Close-up band structures corresponding to the red dashed boxes in panel (b). The color scale and dot size represent the $\langle S_z \rangle$ expectation value. (d) Electrically controlled spin-filter device. A fully spin-polarized current is realized in the device, where opposite spin polarizations are spatially locked to the different conducting edges and can be switched by an out-of-plane electric field.

and 3(c), respectively. We can clearly see a typical energy double-well structure with a low energy barrier of 15 meV per formula unit (meV/f.u.), substantially lower than those of typical perovskite FEs (such as 170 meV/f.u. for $BaTiO_3$ and 335 meV/f.u. for $PbTiO_3$ [83]). Such an ultralow FE switching barrier is favorable for high-speed data writing with low energy cost. The saddle point [$\mathbf{v}_{||} = (0.25, 0.25)$] on the energy surface corresponds to the inversion-symmetric paraelectric (PE) phase, which exhibits an unstable interlayer-sliding phonon mode and can spontaneously transform into the FE phase (Sec. E of SM [58]). Moreover, the spin-resolved topology of the 3D QSHI state survives across the entire FE switching pathway, indicating the robust topology.

Electrically controlled spin filters—To utilize the unique properties of the topological FE insulator, we design an electrically controlled spin-filter device in a bilayer film. Because of the vdW coupling between layers, the bilayer of γ-Bi_4Br_4 can be obtained by exfoliation or molecular beam epitaxy. It is referred to as a π bilayer since the two layers are related by a 180-degree rotation [84]. We systematically investigate the topological edge states of the π bilayer. The crystal and band structures of the FE1 bilayer ribbon are presented in Figs. 4(a)–4(c). Two pairs of edge states are clearly visible within the bulk band gap at each edge, with spin orientations predominantly aligned along the z axis. The interlayer hybridization of these spin-momentum-locked edge states plays a crucial role in determining the spin-current characteristics of the π-bilayer device. On the left edge [left panels of Figs. 4(b) and 4(c)], two pairs of edge states exhibit a *negligible* hybridization gap (less than 1 meV), yielding two forward-propagating spin-up channels and two backward-propagating spin-down channels. By contrast, the right-edge states exhibit a *sizable* hybridization gap [15 meV; right panels of Figs. 4(b) and 4(c)]. This edge-dependent hybridization is further confirmed by first-principles ribbon calculations (Sec. F of SM [58]). These features indicate that the FE1 bilayer functions as a spin filter at low temperature [85]: when an unpolarized current is injected into the ribbon in the forward direction, a purely spin-up-polarized current is generated along a single edge [the left panel of Fig. 4(d)].

Upon application of a z-direction electric field, the bilayer can be switched from the FE1 phase (i.e., spin-up filter) to the FE2 phase (i.e., spin-down filter). The FE2 bilayer ribbon can show spin-filter behavior with opposite spin polarization: the unpolarized current now flows solely along the other edge and becomes purely spin-down polarized, as shown in the right panel of Fig. 4(d). Thus, these results demonstrate an electrically controlled spin-filter device that generates a switchable spin-polarized current.

Conclusion and discussion—In summary, we predict an unreported γ phase of bismuth monohalides Bi_4X_4 and demonstrate that it is an ideal 3D-TFE insulator with a sizable band gap and robust band topology. Although a few 3D topological FE material platforms have been proposed, they are either metallic or require external tuning. By contrast, the new γ-Bi_4X_4 is predicted to be the real material candidate for an intrinsic 3D-TFE insulator, which is highly desirable and timely. Because of the unique vdW stacking and sliding-induced inversion-symmetry breaking, we propose that this γ phase can be identified experimentally by observing the alignment between every other layer in STEM and detecting a nonzero second harmonic generation signal. By surveying various experimental studies on Bi_4X_4, we find that a STEM image of Bi_4Br_4 reported in Ref. [86] strongly supports the γ phase (Sec. G of SM [58]). The spin-resolved topology of the 3D QSHI state is indicated by the nonzero SCN. The computed bulk SHC $\sigma^z_{xy} = 1.925\{(e/2\pi)[1/c]\}$ suggests that the nearly quantized 3D quantum spin Hall effect can be expected in experiment. Moreover, sliding ferroelectricity is found in the 3D topological γ-Bi_4X_4 compound. We suggest that FE switching can be observed experimentally in flakes. Finally, we propose an electrically controlled spin-filter device in a bilayer film capable of producing a switchable spin-polarized current. Overall, the family of γ-Bi_4X_4 can serve as a very promising material platform for the electrically controlled spin-filter device and other electrically controlled, nonvolatile quantum spintronic devices.

Acknowledgments—This work was supported by the National Natural Science Foundation of China under Grant No. 12188101, the National Key R&D Program of China under Grant No. 2022YFA1403800, and the Center for Materials Genome. H. W. acknowledges support from the New Cornerstone Science Foundation through the XPLORER PRIZE.

Data availability—The data that support the findings of this article are publicly available [87].

[1] L. Fu, C. L. Kane, and E. J. Mele, Topological insulators in three dimensions, Phys. Rev. Lett. **98**, 106803 (2007).
[2] M. Z. Hasan and C. L. Kane, Colloquium: Topological insulators, Rev. Mod. Phys. **82**, 3045 (2010).
[3] X.-L. Qi and S.-C. Zhang, Topological insulators and superconductors, Rev. Mod. Phys. **83**, 1057 (2011).
[4] M. König, S. Wiedmann, C. Brüne, A. Roth, H. Buhmann, L. W. Molenkamp, X.-L. Qi, and S.-C. Zhang, Quantum spin Hall insulator state in HgTe quantum wells, Science **318**, 766 (2007).
[5] H. Zhang, C.-X. Liu, X.-L. Qi, X. Dai, Z. Fang, and S.-C. Zhang, Topological insulators in Bi_2Se_3, Bi_2Te_3 and Sb_2Te_3 with a single Dirac cone on the surface, Nat. Phys. **5**, 438 (2009).
[6] S. Nie, L. Xing, R. Jin, W. Xie, Z. Wang, and F. B. Prinz, Topological phases in the $TaSe_3$ compound, Phys. Rev. B **98**, 125143 (2018).
[7] C. Chen *et al.*, Observation of topological electronic structure in quasi-1D superconductor $TaSe_3$, Matter **3**, 2055 (2020).
[8] L. Fu, Topological crystalline insulators, Phys. Rev. Lett. **106**, 106802 (2011).
[9] T. H. Hsieh, H. Lin, J. Liu, W. Duan, A. Bansil, and L. Fu, Topological crystalline insulators in the SnTe material class, Nat. Commun. **3**, 982 (2012).
[10] J. Liu, T. H. Hsieh, P. Wei, W. Duan, J. Moodera, and L. Fu, Spin-filtered edge states with an electrically tunable gap in a two-dimensional topological crystalline insulator, Nat. Mater. **13**, 178 (2014).
[11] J. Han, A. Richardella, S. A. Siddiqui, J. Finley, N. Samarth, and L. Liu, Room-temperature spin-orbit torque switching induced by a topological insulator, Phys. Rev. Lett. **119**, 077702 (2017).
[12] A. R. Mellnik, J. S. Lee, A. Richardella, J. L. Grab, P. J. Mintun, M. H. Fischer, A. Vaezi, A. Manchon, E.-A. Kim, N. Samarth, and D. C. Ralph, Spin-transfer torque generated by a topological insulator, Nature (London) **511**, 449 (2014).
[13] K. Kondou, R. Yoshimi, A. Tsukazaki, Y. Fukuma, J. Matsuno, K. S. Takahashi, M. Kawasaki, Y. Tokura, and Y. Otani, Fermi-level-dependent charge-to-spin current conversion by Dirac surface states of topological insulators, Nat. Phys. **12**, 1027 (2016).
[14] J. Huang, X. Duan, S. Jeon, Y. Kim, J. Zhou, J. Li, and S. Liu, On-demand quantum spin Hall insulators controlled by two-dimensional ferroelectricity, Mater. Horiz. **9**, 1440 (2022).
[15] A. Marrazzo and M. Gibertini, Twist-resilient and robust ferroelectric quantum spin Hall insulators driven by van der Waals interactions, npj 2D Mater. Appl. **6**, 30 (2022).
[16] J. Li, Q. Wu, and H. Weng, Ferroelectric switching of quantum anomalous Hall effects in $MnBi_2Te_4$ films, npj Quantum Mater. **10**, 89 (2025).
[17] S. K. Chakraborty, B. Kundu, B. Nayak, S. P. Dash, and P. K. Sahoo, Challenges and opportunities in 2D heterostructures for electronic and optoelectronic devices, iScience **25**, 103942 (2022).
[18] A. K. Geim and I. V. Grigorieva, Van der Waals heterostructures, Nature (London) **499**, 419 (2013).
[19] Y. Bai, L. Cai, N. Mao, R. Li, Y. Dai, B. Huang, and C. Niu, Doubled quantum spin Hall effect with high-spin Chern number in α-antimonene and α-bismuthene, Phys. Rev. B **105**, 195142 (2022).
[20] J. Gou, H. Bai, X. Zhang, Y. L. Huang, S. Duan, A. Ariando, S. A. Yang, L. Chen, Y. Lu, and A. T. S. Wee, Two-dimensional ferroelectricity in a single-element bismuth monolayer, Nature (London) **617**, 67 (2023).
[21] Y. Lu, W. Xu, M. Zeng, G. Yao, L. Shen, M. Yang, Z. Luo, F. Pan, K. Wu, T. Das, P. He, J. Jiang, J. Martin, Y. P. Feng, H. Lin, and X.-S. Wang, Topological properties determined by atomic buckling in self-assembled ultrathin Bi(110), Nano Lett. **15**, 80 (2015).
[22] Y. Lu, D. Zhou, G. Chang, S. Guan, W. Chen, Y. Jiang, J. Jiang, X.-S. Wang, S. A. Yang, Y. P. Feng, Y. Kawazoe, and

H. Lin, Multiple unpinned Dirac points in group-Va single-layers with phosphorene structure, npj Comput. Mater. **2**, 16011 (2016).
[23] C. Xiao, F. Wang, S. A. Yang, Y. Lu, Y. Feng, and S. Zhang, Elemental ferroelectricity and antiferroelectricity in group-V monolayer, Adv. Funct. Mater. **28**, 1707383 (2018).
[24] S. Zhong, X. Zhang, S. Liu, S. A. Yang, and Y. Lu, Giant and nonanalytic negative piezoelectric response in elemental group-Va ferroelectric monolayers, Phys. Rev. Lett. **131**, 236801 (2023).
[25] S. Liu, Y. Kim, L. Z. Tan, and A. M. Rappe, Strain-induced ferroelectric topological insulator, Nano Lett. **16**, 1663 (2016).
[26] B. Monserrat, J. W. Bennett, K. M. Rabe, and D. Vanderbilt, Antiferroelectric topological insulators in orthorhombic AMgBi compounds ($A = \mathrm{Li, Na, K}$), Phys. Rev. Lett. **119**, 036802 (2017).
[27] D. Di Sante, P. Barone, A. Stroppa, K. F. Garrity, D. Vanderbilt, and S. Picozzi, Intertwined Rashba, Dirac, and Weyl fermions in hexagonal hyperferroelectrics, Phys. Rev. Lett. **117**, 076401 (2016).
[28] E. Plekhanov, P. Barone, D. Di Sante, and S. Picozzi, Engineering relativistic effects in ferroelectric SnTe, Phys. Rev. B **90**, 161108(R) (2014).
[29] L. Li and M. Wu, Binary compound bilayer and multilayer with vertical polarizations: Two-dimensional ferroelectrics, multiferroics, and nanogenerators, ACS Nano **11**, 6382 (2017).
[30] K. Yasuda, X. Wang, K. Watanabe, T. Taniguchi, and P. Jarillo-Herrero, Stacking-engineered ferroelectricity in bilayer boron nitride, Science **372**, 1458 (2021).
[31] J. Ji, G. Yu, C. Xu, and H. J. Xiang, General theory for bilayer stacking ferroelectricity, Phys. Rev. Lett. **130**, 146801 (2023).
[32] Z. Wang, B. J. Wieder, J. Li, B. Yan, and B. A. Bernevig, Higher-order topology, monopole nodal lines, and the origin of large Fermi arcs in transition metal dichalcogenides $X\mathrm{Te}_2$ ($X = \mathrm{Mo, W}$), Phys. Rev. Lett. **123**, 186401 (2019).
[33] Z. Wang, D. Gresch, A. A. Soluyanov, W. Xie, S. Kushwaha, X. Dai, M. Troyer, R. J. Cava, and B. A. Bernevig, MoTe_2: A type-II Weyl topological metal, Phys. Rev. Lett. **117**, 056805 (2016).
[34] A. A. Soluyanov, D. Gresch, Z. Wang, Q. Wu, M. Troyer, X. Dai, and B. A. Bernevig, Type-II Weyl semimetals, Nature (London) **527**, 495 (2015).
[35] P. Sharma, F.-X. Xiang, D.-F. Shao, D. Zhang, E. Y. Tsymbal, A. R. Hamilton, and J. Seidel, A room-temperature ferroelectric semimetal, Sci. Adv. **5**, eaax5080 (2019).
[36] F.-T. Huang, S. Joon Lim, S. Singh, J. Kim, L. Zhang, J.-W. Kim, M.-W. Chu, K. M. Rabe, D. Vanderbilt, and S.-W. Cheong, Polar and phase domain walls with conducting interfacial states in a Weyl semimetal MoTe_2, Nat. Commun. **10**, 4211 (2019).
[37] A. Jindal, A. Saha, Z. Li, T. Taniguchi, K. Watanabe, J. C. Hone, T. Birol, R. M. Fernandes, C. R. Dean, A. N. Pasupathy, and D. A. Rhodes, Coupled ferroelectricity and superconductivity in bilayer T_d-MoTe_2, Nature (London) **613**, 48 (2023).
[38] Z. Fei, W. Zhao, T. A. Palomaki, B. Sun, M. K. Miller, Z. Zhao, J. Yan, X. Xu, and D. H. Cobden, Ferroelectric switching of a two-dimensional metal, Nature (London) **560**, 336 (2018).
[39] H. G. von Schnering, H. von Benda, and C. Kalveram, Wismutmonojodid BiJ, eine Verbindung mit Bi(O) und Bi (II), Z. Anorg. Allg. Chem. **438**, 37 (1978).
[40] R. Noguchi *et al.*, A weak topological insulator state in quasi-one-dimensional bismuth iodide, Nature (London) **566**, 518 (2019).
[41] H. von Benda, A. Simon, and W. Bauhofer, Zur Kenntnis von BiBr und $\mathrm{BiBr}_{1,167}$, Z. Anorg. Allg. Chem. **438**, 53 (1978).
[42] J. Zhong, M. Yang, W. Zhao, K. Zhai, X. Zhen, L. Zhang, D. Mu, Y. Liu, Z. Shi, N. Cheng, W. Zhou, J. Wang, W. Hao, Z. Hu, J. Zhuang, J. Lü, and Y. Du, Coalescence of multiple topological orders in quasi-one-dimensional bismuth halide chains, Nat. Commun. **16**, 1163 (2025).
[43] J.-J. Zhou, W. Feng, C.-C. Liu, S. Guan, and Y. Yao, Large-gap quantum spin Hall insulator in single layer bismuth monobromide $\mathrm{Bi}_4\mathrm{Br}_4$, Nano Lett. **14**, 4767 (2014).
[44] J.-J. Zhou, W. Feng, G.-B. Liu, and Y. Yao, Topological edge states in single- and multi-layer $\mathrm{Bi}_4\mathrm{Br}_4$, New J. Phys. **17**, 015004 (2015).
[45] C.-C. Liu, J.-J. Zhou, Y. Yao, and F. Zhang, Weak topological insulators and composite Weyl semimetals: β-Bi_4X_4 ($X = \mathrm{Br, I}$), Phys. Rev. Lett. **116**, 066801 (2016).
[46] W. Hu, J. Gong, Y. Qiu, L. Yang, J.-J. Zhou, and Y. Yao, Phonons drive the topological phase transition in quasi-one-dimensional $\mathrm{Bi}_4\mathrm{I}_4$, Phys. Rev. B **113**, L201111 (2026).
[47] S. Yu, J. Deng, W. Liu, Y. Zhang, Y. Sun, N. Dhale, S. Li, W. Ma, Z. Wang, P. Wu, Z. Liang, X. Zhang, B. Lv, Z. Wang, Z. Wang, and X. Chen, Observation of robust one-dimensional edge channels in a three-dimensional quantum spin Hall insulator, Phys. Rev. X **14**, 041048 (2024).
[48] J. Huang, S. Li, C. Yoon, J. S. Oh, H. Wu, X. Liu, N. Dhale, Y.-F. Zhou, Y. Guo, Y. Zhang, M. Hashimoto, D. Lu, J. Denlinger, X. Wang, C. N. Lau, R. J. Birgeneau, F. Zhang, B. Lv, and M. Yi, Room-temperature topological phase transition in quasi-one-dimensional material $\mathrm{Bi}_4\mathrm{I}_4$, Phys. Rev. X **11**, 031042 (2021).
[49] M. Yang, W. Zhao, D. Mu, Z. Shi, J. Zhong, Y. Li, Y. Liu, J. Zhong, N. Cheng, W. Zhou, J. Wang, Y. Shi, Y. Sun, W. Hao, L. Yang, J. Zhuang, and Y. Du, Mass acquisition of Dirac fermions in $\mathrm{Bi}_4\mathrm{I}_4$ by spontaneous symmetry breaking, Phys. Rev. Lett. **133**, 256601 (2024).
[50] W. X. Zhao, M. Yang, X. Du, Y. D. Li, K. Y. Zhai, Y. Q. Hu, J. F. Han, Y. Huang, Z. K. Liu, Y. G. Yao, J. C. Zhuang, Y. Du, J. J. Zhou, Y. L. Chen, and L. X. Yang, Topological phase transition in quasi-one-dimensional bismuth iodide $\mathrm{Bi}_4\mathrm{I}_4$, npj Quantum Mater. **9**, 103 (2024).
[51] P. Wang, F. Tang, P. Wang, H. Zhu, C.-W. Cho, J. Wang, X. Du, Y. Shao, and L. Zhang, Quantum transport properties of β-$\mathrm{Bi}_4\mathrm{I}_4$ near and well beyond the extreme quantum limit, Phys. Rev. B **103**, 155201 (2021).
[52] J. Zhong, M. Yang, F. Ye, C. Liu, J. Wang, J. Wang, W. Hao, J. Zhuang, and Y. Du, Facet-dependent electronic quantum diffusion in the high-order topological insulator $\mathrm{Bi}_4\mathrm{Br}_4$, Phys. Rev. Appl. **17**, 064017 (2022).
[53] M. Yang, Y. Liu, W. Zhou, C. Liu, D. Mu, Y. Liu, J. Wang, W. Hao, J. Li, J. Zhong, Y. Du, and J. Zhuang, Large-gap quantum spin Hall state and temperature-induced Lifshitz transition in $\mathrm{Bi}_4\mathrm{Br}_4$, ACS Nano **16**, 3036 (2022).

[54] R. Noguchi *et al.*, Evidence for a higher-order topological insulator in a three-dimensional material built from van der Waals stacking of bismuth-halide chains, Nat. Mater. **20**, 473 (2021).

[55] N. Shumiya *et al.*, Evidence of a room-temperature quantum spin Hall edge state in a higher-order topological insulator, Nat. Mater. **21**, 1111 (2022).

[56] Z. Hu, Y. Zhang, Y. Wang, K. Xiao, X. Li, X.-Y. Yu, C.-C. Liu, Z. Wang, H. Yang, Y. Yao, Q.-K. Xue, and W. Li, Evidence of large-scale and room-temperature stair-stepped quantum spin Hall states in Bi_4Br_4, Nat. Sci. Rev. nwag644 (2026).

[57] Z. Wang, S. Yu, X. Cheng, X. Xiao, W. Ma, F. Quan, H. Song, K. Zhang, Y. Zhang, Y. Ma, W. Liu, P. Yadav, H. Sheng, A. Wang, X. Shi, Z. Wang, Q. Niu, Y. Gao, B. Xiang, J. Liu, Z. Wang, and X. Chen, Atomic-scale spin sensing of a 2D *d*-wave altermagnet via helical tunneling, Nature (London) (2026).

[58] See Supplemental Material at http://link.aps.org/supplemental/10.1103/nwyq-3t1f for computational methods, crystal structures, stability, phonon mode, edge states, and experimental evidence, which includes Refs. [59–74].

[59] P. E. Blöchl, Projector augmented-wave method, Phys. Rev. B **50**, 17953 (1994).

[60] G. Kresse and D. Joubert, From ultrasoft pseudopotentials to the projector augmented-wave method, Phys. Rev. B **59**, 1758 (1999).

[61] G. Kresse and J. Furthmüller, Efficiency of *ab-initio* total energy calculations for metals and semiconductors using a plane-wave basis set, Comput. Mater. Sci. **6**, 15 (1996).

[62] G. Kresse and J. Furthmüller, Efficient iterative schemes for *ab initio* total-energy calculations using a plane-wave basis set, Phys. Rev. B **54**, 11169 (1996).

[63] J. P. Perdew, K. Burke, and M. Ernzerhof, Generalized gradient approximation made simple, Phys. Rev. Lett. **77**, 3865 (1996).

[64] S. Grimme, J. Antony, S. Ehrlich, and H. Krieg, A consistent and accurate *ab initio* parametrization of density functional dispersion correction (DFT-D) for the 94 elements H-Pu, J. Chem. Phys. **132**, 154104 (2010).

[65] S. Grimme, S. Ehrlich, and L. Goerigk, Effect of the damping function in dispersion corrected density functional theory, J. Comput. Chem. **32**, 1456 (2011).

[66] A. Togo and I. Tanaka, First principles phonon calculations in materials science, Scr. Mater. **108**, 1 (2015).

[67] S. Nosé, A unified formulation of the constant temperature molecular dynamics methods, J. Chem. Phys. **81**, 511 (1984).

[68] R. D. King-Smith and D. Vanderbilt, Theory of polarization of crystalline solids, Phys. Rev. B **47**, 1651(R) (1993).

[69] R. Resta, Macroscopic polarization in crystalline dielectrics: The geometric phase approach, Rev. Mod. Phys. **66**, 899 (1994).

[70] A. A. Mostofi, J. R. Yates, G. Pizzi, Y.-S. Lee, I. Souza, D. Vanderbilt, and N. Marzari, An updated version of Wannier90: A tool for obtaining maximally-localised Wannier functions, Comput. Phys. Commun. **185**, 2309 (2014).

[71] N. Marzari, A. A. Mostofi, J. R. Yates, I. Souza, and D. Vanderbilt, Maximally localized Wannier functions: Theory and applications, Rev. Mod. Phys. **84**, 1419 (2012).

[72] Q. Wu, S. Zhang, H.-F. Song, M. Troyer, and A. A. Soluyanov, WannierTools: An open-source software package for novel topological materials, Comput. Phys. Commun. **224**, 405 (2018).

[73] H. Park, A. Onwuli, and A. Walsh, Exploration of crystal chemical space using text-guided generative artificial intelligence, Nat. Commun. **16**, 4379 (2025).

[74] A. Jain, S. P. Ong, G. Hautier, W. Chen, W. D. Richards, S. Dacek, S. Cholia, D. Gunter, D. Skinner, G. Ceder, and K. A. Persson, Commentary: The materials project: A materials genome approach to accelerating materials innovation, APL Mater. **1**, 011002 (2013).

[75] Y. Yang, H. Li, L. Sheng, R. Shen, D. N. Sheng, and D. Y. Xing, Topological phase transitions with and without energy gap closing, New J. Phys. **15**, 083042 (2013).

[76] J. Deng, D. Shao, J. Gao, C. Yue, H. Weng, Z. Fang, and Z. Wang, Twisted nodal wires and three-dimensional quantum spin Hall effect in distorted square-net compounds, Phys. Rev. B **105**, 224103 (2022).

[77] E. Prodan, Robustness of the spin-Chern number, Phys. Rev. B **80**, 125327 (2009).

[78] K.-S. Lin, G. Palumbo, Z. Guo, Y. Hwang, J. Blackburn, D. P. Shoemaker, F. Mahmood, Z. Wang, G. A. Fiete, B. J. Wieder, and B. Bradlyn, Spin-resolved topology and partial axion angles in three-dimensional insulators, Nat. Commun. **15**, 550 (2024).

[79] Y. Xie, H. Sheng, Q. Wu, X. Dai, Z. Fang, H. Weng, and Z. Wang, Nonsymmorphic time-reversal-doubled axion insulators, Phys. Rev. X **16**, 041017 (2026).

[80] J. Sinova, D. Culcer, Q. Niu, N. A. Sinitsyn, T. Jungwirth, and A. H. MacDonald, Universal intrinsic spin Hall effect, Phys. Rev. Lett. **92**, 126603 (2004).

[81] S. Murakami, N. Nagaosa, and S.-C. Zhang, SU(2) non-Abelian holonomy and dissipationless spin current in semiconductors, Phys. Rev. B **69**, 235206 (2004).

[82] X. Ma, C. Liu, W. Ren, and S. A. Nikolaev, Tunable vertical ferroelectricity and domain walls by interlayer sliding in β-ZrI_2, npj Comput. Mater. **7**, 177 (2021).

[83] *Physics of Ferroelectrics: A Modern Perspective*, edited by K. M. Rabe, C. H. Ahn, and J.-M. Triscone, Topics in Applied Physics Vol. 105 (Springer-Verlag, Berlin Heidelberg, 2007).

[84] H. Sheng, Z. Fang, and Z. Wang, Ferroelectric metals in 1T/1T′-phase transition metal dichalcogenide MTe_2 bilayers (M = Pt, Pd, and Ni), Phys. Rev. B **108**, 104109 (2023).

[85] J. Zhou, T. Zhou, S.-g. Cheng, H. Jiang, and Z. Yang, Engineering a topological quantum dot device through planar magnetization in bismuthene, Phys. Rev. B **99**, 195422 (2019).

[86] W. Zhao, M. Yang, R. Xu, X. Du, Y. Li, K. Zhai, C. Peng, D. Pei, H. Gao, Y. Li, L. Xu, J. Han, Y. Huang, Z. Liu, Y. Yao, J. Zhuang, Y. Du, J. Zhou, Y. Chen, and L. Yang, Topological electronic structure and spin texture of quasi-one-dimensional higher-order topological insulator Bi_4Br_4, Nat. Commun. **14**, 8089 (2023).

[87] H. Sheng, S. Zhang, Z. Fang, H. Weng, and Z. Wang, Data for "Three-dimensional topological ferroelectrics" [Dataset], Electronic Laboratory for Material Science, https://matelab.iphy.ac.cn/eln/link.html#/186/B0d2 (2026).